Proceedings of ASME Turbo Expo 2010: Power for Land, Sea and Air
GT2010
June 14-18, 2010, Glasgow, UK

GT2010-22513

3D SIMULATION OF COUPLED FLUID FLOW AND SOLID HEAT CONDUCTION FOR THE CALCULATION OF BLADE WALL TEMPERATURE IN A TURBINE STAGE

Fabien Wlassow
DT/MD/MO
Turbomeca
64511 Bordes Cedex
FRANCE
Email: fabien.wlassow@cerfacs.fr

Florent Duchaine
CFD Team
CERFACS
31057 Toulouse Cedex 1
FRANCE
Email: florent.duchaine@cerfacs.fr

Gilles Leroy
DT/MD/MO
Turbomeca
64511 Bordes Cedex
FRANCE
Email: gilles.leroy@turbomeca.fr

Nicolas Gourdain
CFD Team
CERFACS
31057 Toulouse Cedex 1
FRANCE
Email: gourdain@cerfacs.fr

ABSTRACT

A critical problem in high pressure turbine of modern engine is the vane and blade reliability as it is subjected to high thermal constraints. Actually the flow entering the turbine presents high level of stagnation temperature as well as great radial and circumferential temperature gradients. Considering that a small variation of the blade temperature leads to a strong reduction of its life duration, accurate numerical tools are required for prediction of blade temperature. Because of the complexity of the flow within a turbomachine, the blade wall temperature is heterogeneous and a fluid/solid coupling may improve wall temperature prediction. This study presents a coupling strategy of a Navier Stokes flow solver and a conduction solver to predict blade temperature. Firstly, the method is applied to the well documented NASA C3X configuration. The influence of the fluid/solid interface boundary condition is studied with regards to the wall temperature and heat flux prediction as well as to the computational efficiency. The predicted wall temperature is in good agreement with the experimental results. The method is finally applied to the prediction of the blade temperature of a high pressure turbine representative of a modern engine. Adiabatic and coupled results are compared and discussed.

NOMENCLATURE

A SYMBOLS
C Heat capacity ($J.kg^{-1}.K^{-1}$)
L Characteristic length scale
$\mathcal{N}$ Number of point of the fluid/solid interface
N Number of CHT cycle
P Pressure (Pa)
PS Pressure side
$\mathcal{R}$ CHT calculation convergence criterion
S Surface distance over arc length
SS Suction side
T Temperature (K)
Ts Static temperature (K)
T* Coolant temperature (K)
h Heat transfer coefficient ($W.m^{-2}.K^{-1}$)
k Parameter of the mixed boundary condition
n Number of iterations of the solver
y^+ Normalized wall distance
α Period of exchange between the two codes
Δt Time step of the solver
Φ Heat flux ($W.m^{-2}$)
Γ Fluid/Solid interface
ρ Density ($kg.m^{-3}$)
τ Characteristic time scale (s)

B SUPERSCRIPT
I Point of the fluid/solid interface
n Fluid or solid iteration

C SUBSCRIPT
aw Adiabatic wall
c Convective parameter
f Fluid
i Total variable
s Solid
w Wall

D ACRONYMS
CHT Conjugate Heat Transfer
LES Large Eddy Simulation
RANS Reynolds-Averaged Navier Stokes

INTRODUCTION

In order to increase the thermodynamic efficiency of gas turbine engines, the turbine inlet temperature has been continually increased up to reach levels of the order of magnitude of the high pressure turbine vanes and blades melting temperatures. Moreover because of the mixing within the combustor and its framework characteristic, the temperature and pressure fields at the turbine inlet exhibit azimuthal and radial non-uniformity known as hot streaks. Thus the prediction of the heat load and wall temperature is essential for the estimation of the turbine components life duration. Since experimental data are difficult to collect for real operating conditions, designers often rely on numerical simulation.

Hence many authors studied the effects of hot streaks on turbines. Several experimental studies have been carried out on the effects of inlet total temperature and total pressure profiles [1–4]. Compared with uniform inlet profiles, a modification of the temperature field was observed especially near the hub and tip corners. This modification of the temperature field was ascribed to the secondary flows which are driven by the inlet total pressure gradient [5]. The hot streaks migration in the rotor stage was mainly studied using unsteady Reynolds-Averaged Navier Stokes (RANS) simulations [6, 7] which helped to identify and understand the preferential migration of the hot streak toward the pressure side of the rotor blade. This result was later used by Dorney and Gundy-Burlet [8] and He et al. [9] to reduce the rotor heat load by arranging the clocking between hot streaks and vanes in such a way that the hot streaks impinge on the vanes leading edges.

All these studies have helped to understand the migration of hot streaks in turbine stages and its influence on the turbine heat load, however these simulations are not sufficient to predict the wall temperature of rotor blades. Actually, because of the hot streaks migration, the blade surface temperature varies spatially and temporally. Thus it is not possible to specify *a priori* the blade surface temperature. Hence it is necessary to couple a flow solver with a conduction solver to predict the blade surface temperature. Such calculations are known as Conjugate Heat Transfer (CHT) simulations. Two main approaches were used to envestigate CHT problems in the field of turbomachinery. The first one is a direct coupling where the entire system of equations in the fluid and solid is solved simultaneously by a monolithic solver [10, 11]. The main advantage of this strategy is that the continuity of the temperature and heat flux at the fluid/solid interface is implicitly guaranteed. Luo and Razinski [12] used this approach to predict the metal wall temperature of the NASA C3X vane using different turbulence models and Agostini and Arts [13] investigate the heat transfer in a rib-roughened channel representative of an internal vane cooling system. The second approach consists in solving each set of field equations separately with dedicated solvers that exchange boundary conditions at their interfaces [14–16]. This solution has the advantage to solve fluid and solid equations using existing state-of-the-art codes which have been extensively validated. However it requires to exchange the boundary conditions between the two solvers in an accurate and stable fashion. Hence special attention is required to set up the coupling methodology between the codes. Heselhaus and Vogel [17] attempted such calculations for a turbine cascade and show the difference in wall temperature with an adiabatic simulation. Sondak and Dorney [18] used an unsteady flow solver coupled with an unsteady conduction solver in order to capture the temporal evolution of a rotor blade temperature. More recently Duchaine et al. [19] developed a strategy to couple a LES solver with a conduction solver in a parallel framework.

The present study investigates strategies to couple efficiently RANS and URANS flow solvers with a conduction solver in order to predict turbine blade surface temperature. The influence of the exchanged variables as well as the synchronization between the solvers are studied. The coupling methodology is evaluated on the well documented NASA C3X test case [20] and then applied to a high pressure turbine representative of an actual helicopter engine. For the latter case, two-dimensional inlet total temperature and total pressure fields representative of an combustor exit are imposed and an unsteady RANS flow solver is considered in order to take into account both the migration of hot streaks in the vane passage and in the rotor passage. Firstly the NASA C3X test case is presented. Then the CHT methodology is described. This methodology is assessed with the NASA C3X test case in a third part. Finally, results for a turbine stage are presented.

TEST CASE

The test case used to assess the CHT methodology is the well documented NASA C3X cooled turbine cascade reported by Hylton et al. [20] and presented Fig. 1. The experimental cascade employed three cooled vanes made of ASTM310 stainless steel and the center vane is instrumented for heat transfer and aerodynamic measurements. The vane geometric characteristics and the solid thermal properties are presented respectively in Tab. 1 and 2. The cooling system corresponds to ten holes for which the hole diameter, the averaged coolant temperature and flow rate were measured and are presented in a NASA re-

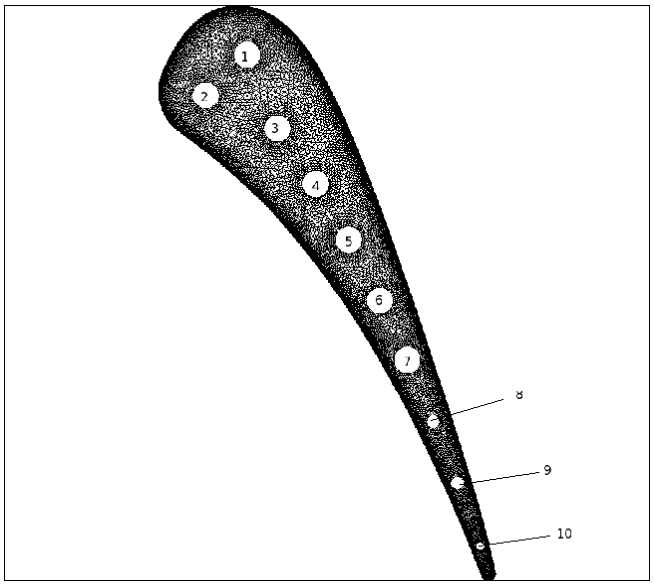

Figure 1. NASA C3X MESH FOR CONDUCTION SIMULATION

Table 1. CASCADE GEOMETRY

Setting angle (°)	59.89
Air exit angle (°)	72.38
Vane height (m)	0.07620
Vane spacing (m)	0.11773
True chord (m)	0.14493
Axial chord (m)	0.07816

Table 2. THERMAL CHARACTERISTICS OF ASTM310

Thermal conductivity ($W.m^{-1}.K^{-1}$)	k_s	$6.811 + 0.020176 * T$
Heat capacity ($J.kg^{-1}.K^{-1}$)	C_s	586.15
Density ($kg.m^{-3}$)	ρ_s	7900.0

port [20]. Associated heat transfer coefficients were calculated from Nusselt number correlation for turbulent flow. The center vane is instrumented with pressure taps and thermocouples. The thermocouples are located in the fully two dimensional region of the vane near midspan and additional thermocouples were installed off midspan to check the 2-D assumption. Pressure taps are located near midspan. Experimental results were obtained over a wide range of operating conditions. The run 158 was selected for this study. The operating conditions are presented in Tab. 3.

Table 3. OPERATING CONDITIONS FOR RUN 158

Inlet Total temperature (K)	808.0
Inlet Total pressure (Pa)	243700.0
Inlet Mach Number	0.17
Outlet Mach Number	0.91
Inlet Turbulence level (%)	8.3

METHODOLOGY

This section presents the methodology used to perform the CHT simulation. The flow and conduction solvers are first presented. Then, the coupling strategy is described.

Flow solver

The flow solver used for this study is the *elsA* software developed by ONERA and CERFACS [21]. This is a finite volume cell centered code that solves the RANS or LES equations on multi-block structured meshes. The *elsA* software is able to take advantage of modern massively parallel platforms [22]. For this study a second order Roe scheme with a Harten entropic correction is used to compute convective fluxes and a second order centered scheme is used for the diffusive fluxes. The two-equation $k-l$ model of Smith [23] is used to compute the eddy viscosity. Local transition criteria such as the Abu-Ghannam and Shaw criterion [24] may be used for transition. For steady flow calculations, an implicit time integration is achieved through a backward Euler scheme coupled with a scalar LU-SSOR method [25].

For the NASA C3X mesh a HOH topology is used. The O block contains 125, 53 and 5 points respectively in the streamwise, pitchwise and spanwise direction. Only few points are used for the spanwise direction since the experiment [20] report a fully 2-D flow. It corresponds to a height of 0.01 m in the spanwise direction. The full domain has 84,885 points (Fig. 2). The average y^+ around the vane is 0.55. 8 power units of an IBM IDATAPLEX system were used for the flow simulation.

Conduction solver

The conduction solver is the AVTP code developed at CERFACS. It solves the transient conduction in solid domains described by the energy conservation. The parallel implementation of AVTP on unstructured grids allows to solve heat conduction on complex geometries. The code takes into account changes of heat capacity and conductivity with temperature using analytical laws. The numerical integration uses either a cell-vertex finite volume 4Δ operator or a finite element Galerkin 2Δ operator [26]. The explicit scheme provides second-order accuracy on hybrid meshes.

A view of the NASA C3X solid mesh is presented on

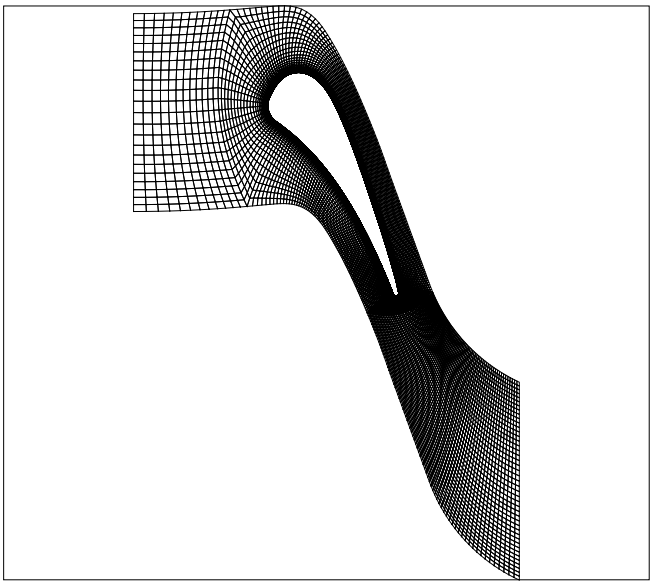

Figure 2. NASA C3X MESH FOR FLOW SIMULATION

Table 4. COOLANT TEMPERATURE AND HEAT TRANSFER COEFFICIENT FOR EACH COOLING HOLE

hole	T (K)	h ($W.m^{-2}.K^{-1}$)
1	358.14	1409
2	359.37	1458
3	349.97	1549
4	351.51	1392
5	342.56	1456
6	371.85	1403
7	351.85	1365
8	385.96	1974
9	413.22	1388
10	454.87	1742

Fig. 1. This mesh contains about 2 millions of tetrahedral cells which is clearly over discretized. However, since the solid conduction computation is fast, this mesh was nevertheless used. The computation was performed using 32 computing units of a IBM IDATAPLEX system. The spanwise dimension of the conduction mesh corresponds to the one of the fluid domain mesh and periodicity is enforced in this direction since the experimental results report a 2-D problem. The choice has been done not to solve a purely 2-D problem as for the two solvers the gain in CPU time between a 2-D and a 3-D problem is relatively small. Moreover, the methodology was developped to handle 3-D problems. Since the internal flow is not solved, the boundary conditions on the cooling holes walls were specified using a Fourier condition based on the coolant temperatures and heat transfer coefficient presented in Tab. 4. The positions of the holes are showed on Fig. 1.

Coupling strategy

The resolution of CHT problems involves taking into account multiple questions. Among them, two main issues were considered for the present work:

- For CHT problems, the way to synchronize the solvers and the frequency of the exchanges between the codes influence the stability as well as restitution time of the computations but they are primarily imposed by the physics of the problem. In fact the ratio between the characteristic time scale of the solid (diffusive time scale τ_s) and fluid (convective time scale τ_f) problems is the key parameter. Hence if the characteristic time scale for the solid and fluid problems are of the same order of magnitude then an unsteady behaviour of the fluid problem may induce an unsteady response of the solid. In that case the codes have to be coupled in a strong way, that is to say, the shared variables have to be exchanged with a time coherence so that an unsteady CHT problem will be described. However if one of the time scale is more than one order of magnitude greater than the other one then code sequencing is sufficient and the CHT calculation will reach a steady state of the coupled problem. The last situation is representative of CHT problems in turbines where the solid time scale is much larger than the fluid one. Hence for the NASA C3X case τ_s and τ_f are defined by Eqn. 2.

$$\tau_s = \frac{\rho_s C_s L_s^2}{k_s} \tag{1}$$

$$\tau_f = \frac{L_f}{U} \tag{2}$$

where L_s is the minimal distance between the solid skin surface and a cooling hole and L_f is the axial chord of the vane. Since $\frac{\tau_s}{\tau_f} = 500$ the solid can be assumed to be in a steady state. Thus code sequencing is sufficient to tackle the coupled heat transfer problems treated within this work. Then the choice of the exchange frequency between the codes is not driven by physical consideration but only by numerical ones. Since a steady flow simulation is considered, there is no physical time coherence for the fluid problem. Thus at each CHT cycle the steady flow simulation will be performed until convergence. On the contrary, an unsteady conduction solver is considered so that there is a physical time coherence within the solid problem and the frequency of exchange of the two codes can be related to τ_s. The frequency of exchange is $\frac{1}{\alpha}$ with α defined by Eqn. 3.

$$\alpha = \frac{n_s \Delta t_s}{\tau_s} \tag{3}$$

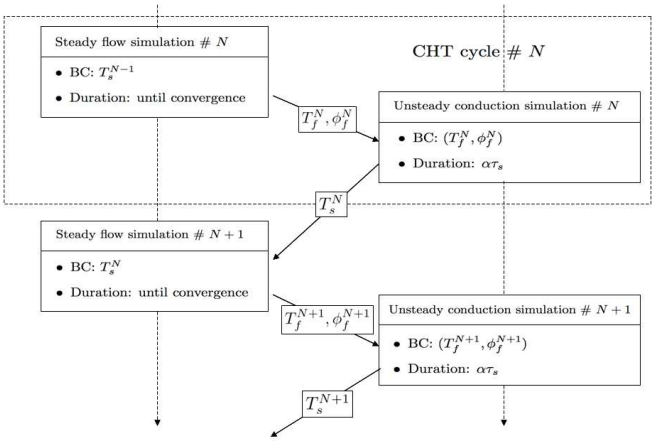

Figure 3. CHT CALCULATION FLOWCHART

where Δt_s and n_s are respectively the conduction solver time step and number of iterations. The flowchart of the CHT calculation associated with this sequential procedure is presented on Fig. 3. Based on this flowchart, the parameter α can be adjusted to improve the convergence rate of the CHT calculation. A small value of α can be regarded as a good thing for convergence because, at each CHT cycle, the conduction solver has no time to reach a final state which is wrong since the boundary conditions have not converged yet. However a great number of CHT cycles will be required since a certain time is needed anyway to let the temperature diffuse in the solid. Moreover when a great number of CHT cycles is considered the cost of the data exchanges may not be negligible anymore.

- The boundary conditions applied to the fluid and solid codes, including the variables shared by the codes, are critical for the precision and stability of the computations.

At a fluid/solid interface Γ_{fs} where thermal properties are discontinuous, heat flux and temperature are continuous. As a consequence, the local heat flux and the temperature must be equal on the interface in the solid and fluid parts:

$$\begin{cases} \phi_f^I = \phi_s^I \\ T_f^I = T_s^I \end{cases}, \quad I \in \Gamma_{fs} \tag{4}$$

with ϕ_f^I, ϕ_s^I the fluid and solid heat fluxes at the interface point I and T_f^I, T_s^I the fluid and solid temperatures at the same location. Thus, the natural variables to share between the codes are ϕ and T at the interfaces. From now on, the notation ^{I} will be dropped for clarity reasons. However shared variables will still be local variables at a point of the interface Γ_{fs}.

Previous studies [27–29] have shown that a good choice to insure stability under some conditions is to impose the heat flux computed in the fluid part to the solid domain through a Neumann boundary condition and the temperature of the solid surface as Dirichlet condition to the fluid frontier. Nevertheless, to reach a converged thermal state, the heat flux computed with the fluid solver will be imposed to the solid boundary on a large number of solid iterations n_s. The imposition of a constant heat flux Φ on a surface S will lead to a linear time derivation of the total energy $E(t)$ of the structure during the interval $t - t_0$ that corresponds to the n_s iterations:

$$E(t) = E(t_0) + \Phi \cdot S \cdot (t - t_0) \tag{5}$$

Such derivations at each update of the solid boundary conditions lead to spurious oscillations of the fluxes and temperatures. This numerical instability often grows and causes a fail of the computation.

Several solutions were proposed in the literature to overcome this type of instability. Sondak and Dorney [18] rewrite Eq. 4 as:

$$\begin{cases} k_f \overrightarrow{grad} T_f = k_s \overrightarrow{grad} T_s \\ T_f \quad = \quad T_s \end{cases} \tag{6}$$

and then estimate the temperature gradient with finite differences. Hence the system of equations can be solved for T and Dirichlet boundary conditions can be imposed on both the fluid and solid solvers. However, when dealing with different kind of grids (structured/unstructured) for the solid and fluid solvers, a first order finite difference expression may not be accurate enough to estimate the temperature gradients at the fluid/solid interface. In this paper it has been chosen to use the heat fluxes calculated with the schemes of each solver in order not to alter their accuracy. Other solutions were used to overcome the problem of numerical instabilities. For instance, one can use a relaxation based on a convective formulation of the heat flux. Indeed, in the heat transfer community, the heat flux at the surface of a structure ϕ_s^n is often express as a Fourier boundary condition:

$$\phi_s^n = h_c(T_s^n - T_c), with \;\; n = 1, n_s \tag{7}$$

with h_c and T_c are the convective heat transfer coefficient and convective temperature respectively. In this formulation, the flux ϕ_s^n and the temperature T_s^n evolve during the iterations leading to the convergence to a steady state between two consecutive updates of T_c and h_c. The convective parameters are determined with the heat flux computed in the fluid ϕ_f and the temperature of the wall surface T_f:

$$h_c(T_f - T_c) = \phi_f \tag{8}$$

Eqn. 8 must be augmented by a way to determine either h_c or T_c. The idea is to fix h_c or T_c and then to determine the corresponding value of T_c or h_c with Eqn. 8. Generally T_c is chosen as the bulk temperature.

For turbomachinery applications, the evolution of the flow field and the boundary layer along the blade prevent a trivial determination of the convective parameters. Instead of using the

total inlet temperature T_{t0}, T_c can be approximated by T_{aw} which represents the surface temperature of a perfectly insulated surface and it is obtained from an adiabatic flow simulation. The main problem when using a given temperature T_c and then using Eqn. 8 to determine h_c is that the procedure can give negative values of the heat transfer coefficient. These non physical values of h_c may lead the computation to fail due to numerical instabilities. In order to avoid negative values of h_c, one can choose to fix the heat transfer coefficient and compute T_c with Eqn. 8. The heat transfer coefficient depends on several parameters but primarily on the thickness and nature of the boundary layer. Indeed, thin boundary layers conduct more heat that thick ones. Turbulent boundary layers transfer more heat per unit of thickness than do laminar ones [30]. Assuming that local h_c is only a function of the aerodynamic field, its determination remains not trivial. From experimental point of view, measurement methods of detailed heat transfer coefficient involve heat-mass transfer analogy, liquid crystal and infrared thermography [31–33]. Numerical prediction with CFD solvers of h_c requires several numerical simulations of the flow field and/or experimental data [32, 34].

Another solution consists in rewriting the continuity of heat flux and temperature across the interface (Eqn. 4) in the following form:

$$\begin{cases} T_f = T_s \\ \phi_f + kT_f = \phi_s + kT_s \end{cases} \quad (9)$$

with k a numerical relaxation parameter. The resulting boundary condition for the structure, called mixed condition, looks :

$$\phi_s^n = \phi_f + k(T_f - T_s^n), with \;\; n = 1, n_s \quad (10)$$

As underlined in the case of the Fourier condition (Eqn. 7), both ϕ_s^n and T_s^n of the mixed formulation converge to a steady state between two consecutive updates of ϕ_f and T_f. The stability of the mixed condition for the solid domain used in conjunction with Dirichlet boundary temperature for the fluid depends on the value of k (when k tends to 0, the mixed formulation tends to the Neumann condition) and on the exchange frequency. Note that at convergence, $T_f = T_s^n$ so that the mixed condition tends to the thermal equilibrium given by Eqn. 4.

The boundary conditions for the coupled problem tested during this work are listed in Table 5. The objective was to check the unicity of the solution obtained with different sets of boundary conditions in order to choose the best suited for the industrial case.

The convergence is monitored on the criterion $\mathcal{R}$, defined by Eqn. 11 which control the evolution of the temperature of Γ_{fs} between two CHT cycle N and $N+1$.

$$\mathcal{R} = \frac{|T_s^{N+1} - T_s^N|_{max}}{\frac{1}{\mathcal{N}} \sum_{i=1}^{\mathcal{N}} T_s^{N+1}} \quad (11)$$

Since the flow and conduction solvers use different meshes three dimensional linear interpolations are used when the shared variables are exchanged.

APPLICATION TO THE ACADEMIC NASA C3X CASE

Methodology

The coupling strategy for CHT problems is assessed on the NASA C3X case. Firstly, the four cases of boundary conditions from Tab. 5 are evaluated and compared. The results obtained for the different boundary conditions for the wall temperature and the convective heat transfer coefficient are presented Fig. 4. For comparability, the convective heat transfer coefficient presented for all boundary conditions is calculated with $T_{ref} = 811$K. One

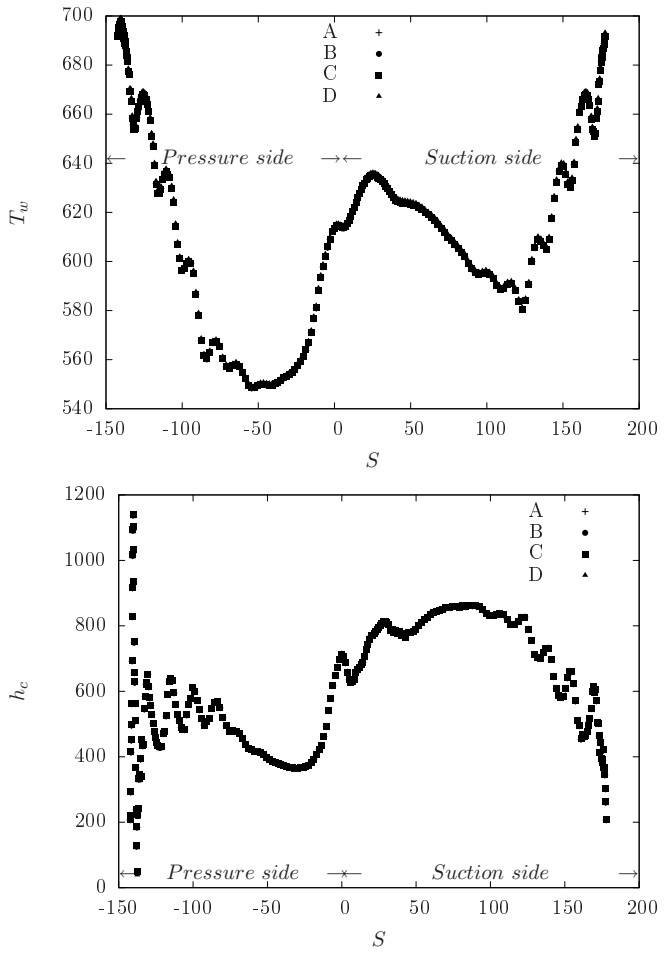

Figure 4. BOUNDARY CONDITION INFLUENCE

can see that all boundary conditions give the same results so that the choice of the boundary condition will be based only on practical and computational efficiency criteria. Hence the mixed condition is preferred as no preliminary computations or experimental study is required as for the Fourier condition with T_{aw} as reference temperature or a fixed local convective heat flux coefficient

Table 5. BOUNDARY CONDITIONS FOR CHT PROBLEMS

Fluid		Solid		Case
Dirichlet	$T_f^n = T_s$	Fourier:	$\phi_s^n = \frac{\phi_f}{T_{ref}-T_f}(T_s^n - T_{ref})$	A
		Fourier:	$\phi_s^n = \frac{\phi_f}{T_{aw}-T_f}(T_s^n - T_{aw})$	B
		Fourier:	$\phi_s^n = h_{ref}(T_s^n - T_f)$	C
		Mixed:	$\phi_s^n = \phi_f + k(T_f - T_s^n)$	D

and no question about the reference parameters is raised. Figure 5 shows the convergence criterion for all type of boundary condition plotted (in logscale) against the number of CHT cycles. It shows that the convergence is the same for the four kinds of boundary condition. The mixed boundary condition parameter k used for this comparison is $k = 100$. As explain below, this value of k gives almost the best convergence rate as maintaining stability.

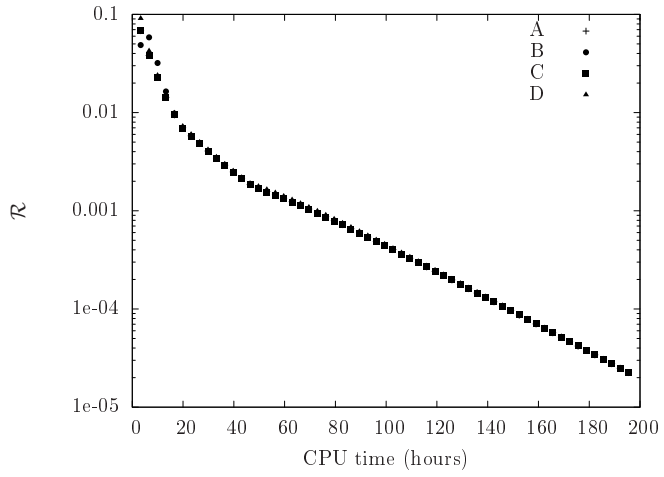

Figure 5. CONVERGENCE OF THE CHT CALCULATION

The parameter k of the mixed boundary condition can be adjusted in order to accelerate the convergence while maintaining the stability of the computations. One can observe that when this parameter decreases, the convergence rate increases. However too small values of k can lead to an unstable coupled system when used with unsuitable exchange frequency [19,28,29]. Four different values of k (50, 500, 5000 and 50000) were tested. Figure 6 shows the convergence rate for these four cases and one can verify that the case $k = 50$ converges more rapidly even if the gain compared with the case $k = 500$ is small. The convergence acceleration when decreasing k is not linear and for small values of k, typically lower than 500, the convergence rates are of the same order magnitude.

The influence of the exchange frequency, defined by Eqn. 3,

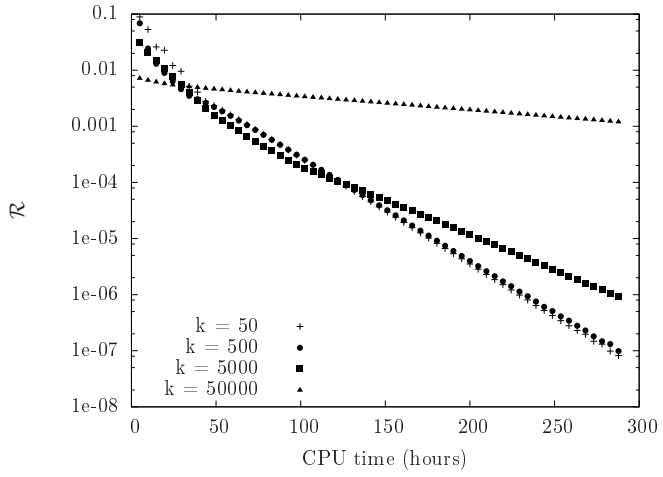

Figure 6. INFLUENCE OF k ON THE CHT SIMULATION CONVERGENCE

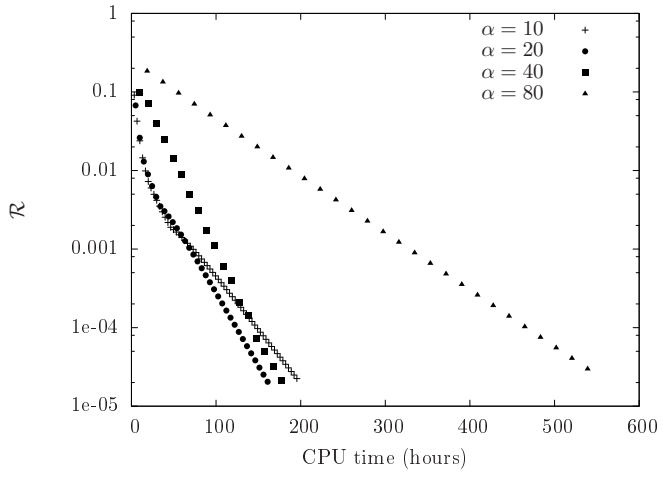

Figure 7. INFLUENCE OF α ON THE CHT SIMULATION CONVERGENCE

was also evaluated by changing the number of iterations of the conduction solver. Four cases were studied : $\alpha = 10$, 20, 40 and 80. Figure 7 shows the convergence of the CHT calculations for these four value of α. At the beginning of the CHT computation, the convergence rate is faster with small value of α. At that point,

the shared variables are wrong with regards to the converged state. So it is important to often update them in order to avoid wasting computational time solving a problem with inaccurate boundary conditions and so to speed up the convergence. However one can see that when $\mathcal{R}$ has reach a level of 10^{-4} the convergence rate starts being faster for medium value of α. The reason is that now the value of the shared variables is closed to the converged state and the information imposed through the boundary conditions has to propagate within the solid domain. So a greater number of iterations is required at each CHT cycle for the conduction solver. For $\alpha = 80$ the computation is inefficient because too much time is spend for the conduction calculation. Based on this study, it may be interesting for computational efficiency to adjust the parameter α in function of the convergence criterion during the computation.

Comparisons with experimental results

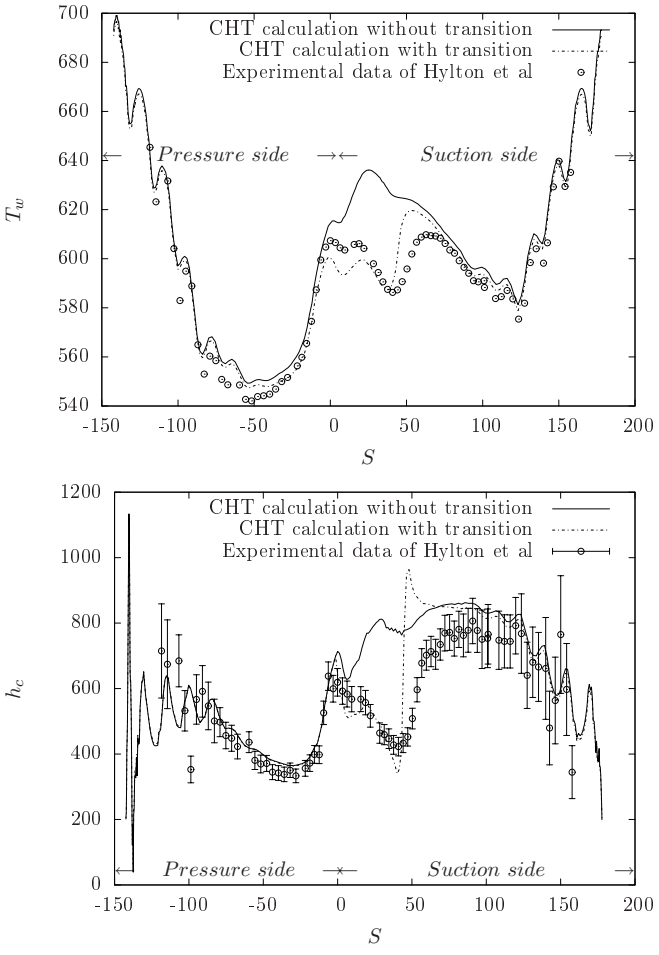

Figure 8. COMPARISON WITH EXPERIMENTAL DATA

Figures 8 presents the results of the CHT calculation compared with the experimental data of Hylton et al. [20]. As for the experimental results, the presented convective heat transfer coefficient is based on a reference temperature $T_{ref} = 811$K. The error bars on the onvective heat transfer coefficient plot indicate the measurements uncertainties. One can observe, near the trailing edge large fluctuations in both wall temperature and heat transfer coefficient. These fluctuations are due to the presence of the cooling holes. These fluctuations are also observed on the experimental results for the wall temperature distribution. For the main part of the blade, the CHT calculation results are in a fair agreement with the experimental data. Nevertheless, a discrepancy is observed on the pressure side near the leading edge. In fact, the RANS turbulent model assumes a fully turbulent boundary layer, however it is clear from the convective heat flux coefficient that laminar to turbulent transition occurs on the pressure side of the blade. Since this transition is not taking into account, the heat fluxes are over predicted in the laminar region, which in turn lead to a over prediction of the temperature. In that region the maximum relative error between computed and experimental temperatures is about 7%. However in the turbulent region the relative error does not exceed 2%. In order to take into account the transition, a correlation criteria [24] was used in the flow solver to locate the transition point and to improve the results of the CHT calculation. The results obtained with transition are also presented Fig. 8 and although the transition is predicted too early, the temperature prediction is improved. Now the maximum relative error on temperature is around 3% in the laminar region and 1% in the turbulent region.

APPLICATION TO AN HELICOPTER TURBINE ROTOR BLADE

Set up of the CHT calculation

The CHT calculation is now applied to an helicopter high pressure turbine. This is a high loaded transonic turbine. For this application the solid can be considered in a steady state ($\frac{\tau_s}{\tau_f} = 4000$). Hence as for the NASA C3X case code sequencing and mixed boundary conditions are used to couple the flow and conduction solvers. The coupled surfaces are the rotor blade profile and tip.

For the flow calculation, the whole turbine stage is considered. To take into account the hot streak migration within the vane passage, a 2D boundary condition including total temperature and total pressure profiles is applied at the inlet of the domain. This boundary condition was extracted from a RANS simulation of a combustion chamber. To capture hot streak migration in the rotor stage, an unsteady flow simulation is considered. For this unsteady flow calculation a Dual Time Stepping scheme is used [35] and the time marching of the inner loop is achieved in the same way than the steady flow calculation. The number of sub-iterations for the inner loop is chosen to ensure a reduction of two orders for the density residual magnitude. The use of phase-lag [36, 37] boundary conditions at the rows interface and on the periodic boundaries enables to consider only a single blade passage of each row for unsteady flow calculation. For memory consideration, only the Fourier coefficients are stored at the rows interface and periodic boundaries. The physical time

step is chosen so that 200 iterations and 510 iterations are set to solve the blade passing frequency of the opposite row respectively in the stator and rotor frame of reference. For the flow, one CHT cycle corresponds to the time required for the rotor blade to traverse the vane passage. The variables shared by the flow solver with the conduction code are $< T_f >$ *and* $< \phi_f >$, where $<>$ denotes time averaged quantities over one CHT cycle. Thanks to the phase-lag method, only one vane passage and one rotor passage are considered, each meshed using a O6H topology. 175, 49 and 89 points are present in the vane mesh respectively in the streamwise, pitchwise and spanwise direction and 109, 49 and 109 for the rotor mesh with 33 points in the radial tip gap. The whole mesh contains 3.5 millions of nodes and the average y^+ is 0.53. A view of the mesh is presented on Fig. 9. The fluid flow calculation was initialized with an unsteady RANS adiabatic solution in order to save the time required for the periodic flow to establish.

For the solid part only the rotor blade is considered. This is an uncooled blade with a fir-tree blade root which is considered for the conduction simulation. It is important to consider the fir-tree root, as a part of the heat fluxes exchanged with the flow will exit through the root. The bottom of the fir-root is set as an isothermal surface. Except the isothermal and the coupled boundaries, every other surfaces are considered adiabatic. Actually, for the real case, the fir-root side surfaces are exchanging heat with the rest of the engine. To model this phenomenon, it would require to simulate the whole system since the thermal conditions here are not known. So it has been assumed that all the heat transfered from the fluid to the hub surface is then transfered to the rest of the engine through the fir-root side surface which means that the heat flux budget between these surfaces is zero. Thus the fir-root side surface and the hub are set as adiabatic surfaces. The mesh for this blade contains 190 077 tetrahedral cells. Most of the cells are located in the blade profile so that the number of elements used to discretize the blade surface for both the flow and the conduction solver are close. In fact, for the blade surface there are 16 159 triangular elements on the solid mesh

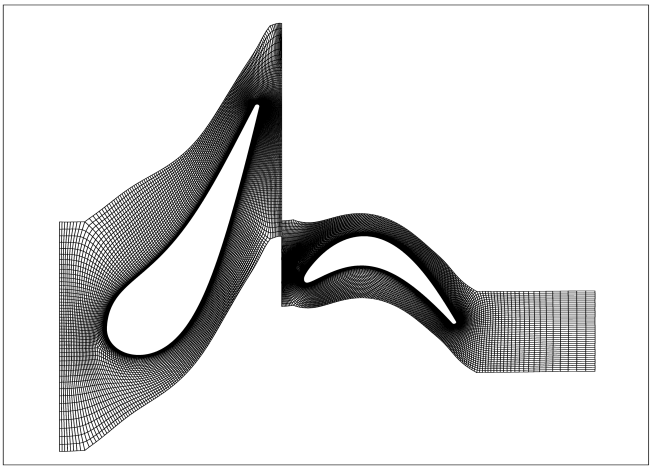

Figure 9. MESH OF THE ONE STAGE TURBINE

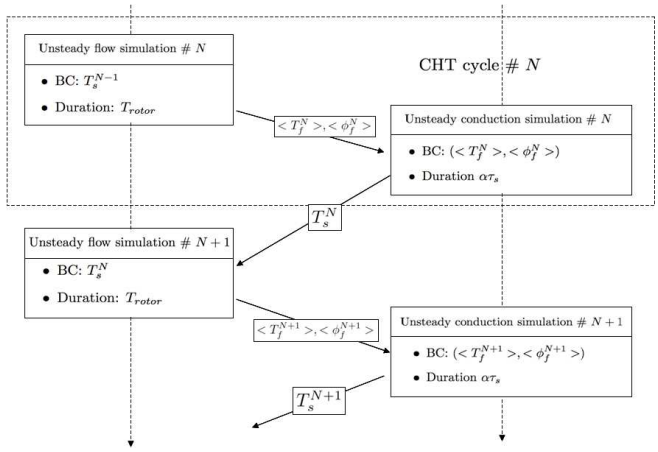

Figure 10. TURBINE STAGE CHT CALCULATION FLOWCHART

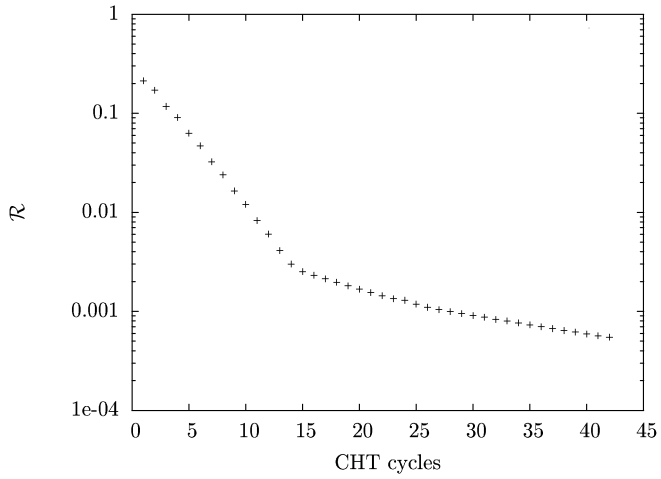

Figure 11. CONVERGENCE OF THE CHT CALCULATION OF THE ROTOR BLADE

and 16 125 quads on the fluid mesh. Thus, errors due to the linear interpolations are reduced. Figure 10 sums up the flowchart of the CHT calculation of the high pressure turbine. The convergence was monitored for the flow and conduction solvers as well as for the coupled interface. For the flow solver, the mass-flow rates and static temperatures at the inlet and outlet of each row were analysed using windowed Fourier transform. The time evolution of the energy spectrum and harmonic amplitudes was monitored to verify a periodic state was reached. For the conduction solver, the time evolution of the minnimum, maximum and average temperature was observed until a steady state was reached. Finally, the criterion $\mathcal{R}$ (Eqn. 11) was supervised until it reaches 10^{-3} (Fig. 11). About 40 CHT cycles were necessary to converge the coupled interface which represents about 2000 CPU hours on the IBM IDATAPLEX system.

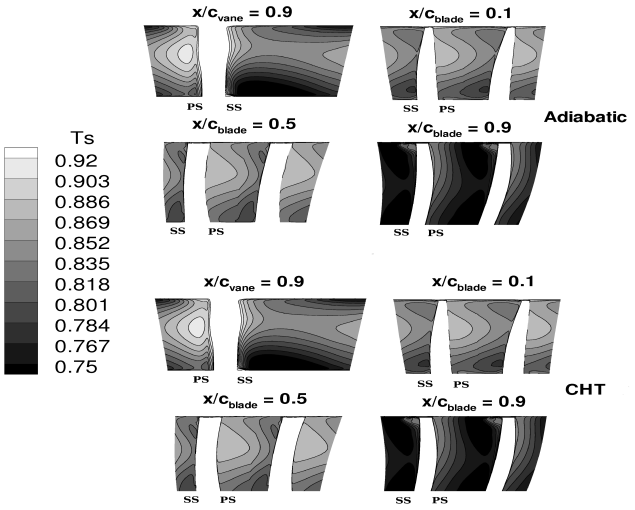

Figure 12. STATIC TEMPERATURE IN THE TURBINE STAGE - TOP: ADIABATIC SIMULATION, BOTTOM: CHT SIMULATION

Results

Figure 12 shows the hot streak migration within the turbine stage at 4 different axial planes. The typical effects of hot streak migration are observed. Actually, a radial migration along the vane span and towards the shroud is observed in the vane passage. In the rotor passage the preferential migration of hot fluid towards the pressure side, the segregation effect, is captured as well as the redistribution of hot fluid on suction side due to the tip leakage flow near le trailing edge. The results are compared with those of an adiabatic wall simulation. The consideration of the solid in the problem does not really influences the hot streak migration as shown by Fig. 12. Only slight modifications of the fluid temperature field are observed, in particular close to the pressure side of the rotor blade. For the CHT case, the radial extension of the hot streak near the pressure side of the rotor blade is slightly reduced. In fact, modifications of the fluid temperature field are observed in thermal boundary layer and close to it but not in the middle of the passage. However the influence on the wall blade temperature is important. Figure 13 shows the relative difference the adiabatic wall temperature and the wall temperature predicted by the CHT simulation. This difference is defined by Eqn. 12.

$$\Delta T/T = \frac{T_{CHT} - T_{aw}}{T_{CHT}} \tag{12}$$

The average temperature of the blade is about 1.9% cooler for the CHT simulation. It may represent a great reduction of the blade's life duration. However the cooling of the blade is heterogenous. Actually, the CHT calculation predicts a lower wall temperature near the hub mainly because the heat is transported in the fir-tree of the blade. Around the blade profile, the CHT calculation predicts higher temperatures for the region where the blade is thin, and lower temperatures where the blade is thicker,

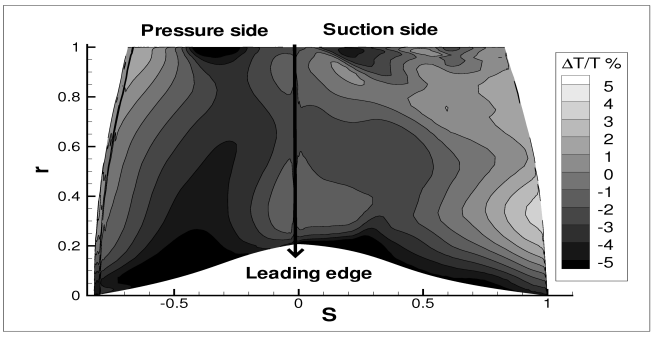

Figure 13. RELATIVE DIFFERENCE BETWEEN WALL TEMPERATURE PREDICTED BY AN ADIABATIC AND A CHT CALCULATION

obviously since the temperature will diffuse more where the solid is thicker.

CONCLUSION

A coupling strategy used to handle CHT problems typical of high pressure turbine cases was described. As the characteristic time scale of the solid is several order of magnitude greater than the one of the fluid, the solid is considered as in a steady state and only code sequencing is considered.

For the coupling methodology the choice of the fluid/solid boundary condition was particularly studied on the well documented NASA C3X case. Three different Fourier boundary conditions, based on different reference temperatures or convective heat transfer coefficients, and a mixed boundary condition were compared. It has been shown that these boundary conditions do not influence the final prediction of the wall vane temperature. However for Fourier type boundary conditions, the choice of a reference temperature or convective heat transfer coefficient is not straightforward and may lead to non-physical behaviours and often requires additional computations. Thus the mixed boundary condition was chosen for the second part of the study. Computational time reduction can be achieved by reducing the parameter k of the mixed boundary condition, however below 500 no real gain is obtained. Finally, the influence of the exchange frequency between the flow and the conduction solver was studied. At the beginning of the CHT calculation, a high exchange frequency is required so that the correction enforced on the heat flux and temperature at each CHT cycle is not too important. However, when the solution has already started to converge the exchange frequency can be reduce to let time for the temperature to diffuse within the solid.

The results of the CHT calculation for the NASA C3X case concerning the wall temperature and the convective heat transfer coefficient were compared with experimental data, showing good agreement. The results have been improved by taking into account boundary layer transition in the flow solver. The average error was around 1% with a maximum of 3% near the leading edge when the transition was taken into account. The CHT methodology was then applied to a turbine rotor blade. For this case, the whole turbine stage was considered in the flow solver

using an unsteady RANS approach in order to capture hot streak migration and to predict a realistic blade temperature distribution. The comparison with a temperature distribution resulting from an adiabatic simulation shows differences that are locally more than 5% which is important for the life duration prediction of the blade.

The CHT strategy can now be used to study in more detail the influence of coolant injections in high turbine pressures and their influence on the blade temperature. The coolant injections have only to be taken into account by the flow solver and the CHT strategy can be applied and give more realistic results than a simple adiabatic flow simulation. One major assumption in this work is that the solid is in a steady state with regards to the fluid. In order to validate the choice of code sequencing, further studies would include unsteady coupling strategy were the fluid and solid solvers will be coupled with time coherence.

ACKNOWLEDGMENT

The authors are grateful to Turbomeca for permission to publish results on their configurations and for their support in this study. Special thanks to the CERFACS - CFD Team for developing efficient numerical methods for the elsA and AVTP softwares as well as for their availability for discussions concerning numerical methods. The authors are also grateful to the *elsA* software team (ONERA).

REFERENCES

[1] Schwab, J. R., Stabe, R. G., and Whitney, W. J., 1983. "Analytical and experimental study of flow through an axial turbine stage with a nonuniform inlet radial temperature profile". *AIAA Paper 83-1175*.

[2] Stabe, R. G., Whitney, W. J., and Moffitt, T. P., 1984. "Performance of a high-work low aspect ratio turbine with a realistic inlet radial temperature profile". *AIAA Paper 84-1161*.

[3] Barringer, M., Thole, K., Polanka, M., Clark, J., and Koch, P., 2009. "Migration of combustor exit profiles through high pressure turbine vanes". *J. Turbomach.,* ***131***, April, pp. 021010–10.

[4] Barringer, M., Thole, K., and Polanka, M., 2009. "An experimental study of combustor exit profile shapes on endwall heat transfer in high pressure turbine". *J. Turbomach.,* ***131***, April, pp. 021009–10.

[5] Hawthrone, W. R., 1951. "Secondary circulation in fluid flow". *Proc. R. Soc. London, Ser. A,* ***206***, pp. 374–387.

[6] Dorney, D., Davis, R., and Edwards, D., 1992. "Unsteady analysis of hot streak migration in a turbine stage". *J. Propul. Power,* ***8***, pp. 520–529.

[7] Takahashi, R., and Ni, R.-H., 1991. "Unsteady hot streak migration through a 1 1/2-stage turbine". In AIAA Paper, no. 91-3382.

[8] Dorney, D., and Gundy-Burlet, K., 1996. "Hot-streak clocking effects in a 1-1/2 stage turbine". *J. Prop. Power,* ***12***, pp. 619–620.

[9] He, L., Menshikova, V., and Haller, B. R., 2004. "Influence of hot streak circumferential length-scale in transonic turbine stage". In ASME TURBO EXPO 2004: International Gas Turbine & Aeroengine Congress & Exhibition, no. GT2004-53370.

[10] Kao, K. H., and Liou, M. S., 1997. "Application of chimera/unstructured hybrid grids for conjugate heat transfer". *AIAA Journal ,* ***35***(9), pp. 1472–1478.

[11] Han, Z. X., Dennis, B., and Dulikravich, G., 2001. "Simultaneous prediction of external flow-field and temperature in internally cooled 3-d turbine blode material". *Int. J. Turbo Jet-Eng. ,* ***18***, pp. 47–58.

[12] Luo, J., and Razinsky, E. H., 2007. "Conjugate heat transfer analysis of a cooled turbine vane using the v2f turbulence model". *J. Turbomach.,* ***129***(4), pp. 773–781.

[13] Agostini, F., and Arts, T., 2005. "Conjugate heat transfer investigation of rib-roughened cooling channels". In Proceedings of ASME Turbo Expo 2005, no. ASME Paper GT2005-68116.

[14] Montenay, A., Paté, L., and Duboué, J. M., 2000. "Conjugate heat transfer analysis of an engine internal cavity". In Proceedings of ASME Turbo Expo 2000, no. ASME Paper 2000-GT-282.

[15] Verdicchio, J., Chew, J., and Hills, N., 2001. "Coupled fluid/solid heat transfer computation for turbine discs". In Proceedings of ASME Turbo Expo 2001, no. ASME Paper 2001-GT-0205.

[16] Amaral, S., Verstraete, T., den Braembussche, R. V., and Arts, T., 2010. "Design and optimization of the internal cooling channels of a high pressure turbine blade - part i: Methodology". *J. Turbomach.,* ***132***(021013).

[17] Heselhaus, A., and Vogel, D. T., 1995. "Numerical simulation of turbine blade cooling with respect to blade heat conduction and inlet temperature profiles". In ASME, SAE, and ASEE, Joint Propulsion Conference and Exhibit, 31st, no. AIAA-1995-3041.

[18] Sondak, D. L., and Dorney, D. J., 2000. "Simulation of coupled unsteady flow and heat conduction in turbine stage". *J. Propul. Power,* ***16***(6), pp. 1141–1148.

[19] Duchaine, F., Mendez, S., Nicoud, F., Corpron, A., Moureau, V., and Poinsot, T., 2009. "Coupling heat transfer solvers and large eddy simulations for combustion applications". *Int. Journ. of Heat and Fluid Flow,* ***30***(6), December, pp. 1129–1141.

[20] Hylton, L., Mihelc, M., Turner, E., Nealy, D., and York, R., 1983. Analytical and experimental evaluation of the heat transfer distribution over the surfaces of turbine vanes. Tech. Rep. CR 168015, NASA.

[21] Cambier, L., and Veuillot, J., 2008. "Status of the elsa cfd software for flow simulation and multidisciplinary applications". In AIAA, Aerospace Sciences Meeting and Exhibit, 46 th, AIAA 2008-664.

[22] Gourdain, N., Montagnac, M., Wlassow, F., and Gazaix, M., to be published. "High performance computing to simulate large scale industrial flows in multistage compressors". *Int. Journal of High Performance Computing*.

[23] Smith, B., 1990. "The k - kl turbulence model and wall layer model for compressible flows". In AIAA Paper, no. 90-1483, 21st Fluid and Plasma Dynamics Conference.
[24] Abu-Ghannam, B. J., and Shaw, R., 1980. "Natural transition of boundary layers. the effects of turbulence, pressure gradient, and flow history". *J. Mech. Engr. Science,* ***22***(5), pp. 213–228.
[25] Yoon, S., and Jameson, A., 1987. "An LU-SSOR Scheme for the Euler and Navier-Stokes Equations". In AIAA 25th Aerospace Sciences Meeting, no. AIAA-87-0600.
[26] Colin, O., and Rudgyard, M., 2000. "Development of high-order taylor-galerkin schemes for unsteady calculations". *J. Comput. Phys. ,* ***162***(2), pp. 338–371.
[27] Giles, M. B., 1997. "Stability analysis of numerical interface conditions in fluid-structure thermal analysis". *Int. J. Numer. Meth. Fluids ,* ***25***(4), pp. 421–436.
[28] Chemin, S., 2006. "Étude des interactions thermiques fluides-structure par un couplage de codes de calcul". PhD thesis, Université de Reims Champagne-Ardenne.
[29] Radenac, E., 2006. "Développement et validation d'une méthode numérique pour le couplage fluide structure en aérothermique instationnaire". PhD thesis, Université Paul Sabatier - Toulouse.
[30] Taine, J., and Petit, J.-P., 1995. *Cours et données de base. Transferts thermiques. Mécanique des fluides anisotherme*. Ed. DUNOD.
[31] Han, J. C., Dutta, S., and Ekkad, S. V., 2000. *Gas Turbine Heat Transfer and Cooling Technology*. Taylor & Francis, New York, NY, USA.
[32] Dunn, M. G., 2001. "Convective heat transfer and aerodynamics in axial flow turbines". *J. Turbomach.,* ***123***, pp. 637–686.
[33] Newton, P. J., Lock, G. D., Krishnababu, S. K., Hodson, H. P., Dawes, W. N., Hannis, J., and Whitney, C., 2006. "Heat transfer and aerodynamics of turbine blade tips in a linear cascade". *J. Turbomach.,* ***128***(2), pp. 300–310.
[34] Ameri, A. A., and Bunker, R. S., 2000. "Heat transfer and flow on the first-stage blade tip of a power generation gas turbine: Part 2 - simulation results". *J. Turbomach.,* ***122***, pp. 272–277.
[35] Jameson, A., 1991. "Time Dependent Calculations Using Multigrid, with Applications to Unsteady Flows Past Airfoils and Wings". In AIAA 10th Computational Fluid Dynamics Conference, no. AIAA-91-1596.
[36] He, L., 1990. "An euler solution for unsteady flows around oscillating blades". *Journal of Turbomachinery,* ***112***(4), pp. 714–722.
[37] Erdos, J., Alzner, E., and McNally, W., 1977. "Numerical Solution of Periodic Transonic Flow Through a Fan Stage". *AIAA Journal,* ***15***, pp. 1559–1568.